

# MSF: Efficient Diffusion Model Via Multi-Scale Latent Factorize

Haohang Xu<sup>1\*</sup> Longyu Chen<sup>1,2\*</sup> Shuangrui Ding<sup>3</sup> Yilin Gao<sup>1,4</sup>  
 Dongsheng Jiang<sup>1</sup> Yin Li<sup>1</sup> Shugong Xu<sup>4</sup> Junqing Yu<sup>2</sup> Wei Yang<sup>2</sup>  
<sup>1</sup> Huawei Inc. <sup>2</sup> Huazhong University of Science & Technology  
<sup>3</sup> The Chinese University of Hong Kong <sup>4</sup> Shanghai University

## Abstract

*Diffusion-based generative models have achieved remarkable progress in visual content generation. However, traditional diffusion models directly denoise the entire image from noisy inputs, disregarding the hierarchical structure present in visual signals. This method is computationally intensive, especially for high-resolution image generation. Signal processing often leverages hierarchical decompositions; for instance, Fourier analysis decomposes signals by frequency, while wavelet analysis captures localized frequency components, reflecting both spatial and frequency information simultaneously. Inspired by these principles, we propose a multi-scale diffusion framework that generates hierarchical visual representations, which are subsequently integrated to form the final output. The diffusion model’s target, whether raw RGB pixels or latent features from a Variational Autoencoder (VAE), is divided into multiple components that each capture distinct spatial levels. The low-resolution component contains the primary informative signal, while higher-resolution components add high-frequency details, such as texture. This approach divides image generation into two stages: producing a low-resolution base signal, followed by a high-resolution residual signal. Both stages can be effectively modeled using simpler, lightweight transformer architectures compared to full-resolution generation. This decomposition is conceptually similar to wavelet decomposition but offers a more streamlined and intuitive design. Our method, termed MSF (short for Multi-Scale Factorization), achieves an FID of 2.2 and an IS of 255.4 on the ImageNet  $256 \times 256$  benchmark, reducing computational costs by 50% compared to baseline methods.*

## 1. Introduction

Diffusion models have recently demonstrated impressive performance across a range of generative tasks, including

image [11, 29, 39, 43], video [2, 3, 21, 45, 53], and audio synthesis [9, 24, 28, 40]. These models iteratively transform random Gaussian noise into high-quality outputs by progressively applying denoising steps. Despite their effectiveness, conventional diffusion models operate directly on high-resolution images throughout the denoising process, which imposes significant computational demands due to the multi-step reverse sampling required. This issue is especially pronounced in architectures with  $O(n^2)$  computational complexity, such as DiT [38] and FiT [34, 50], where the computational overhead becomes prohibitive.

A series of recent studies [25, 32, 33, 54, 55] aim to accelerate the reverse sampling process by employing deterministic Differential Equation solvers. These methods reformulate the reverse diffusion process as either a Stochastic Differential Equation (SDE) [47] or an Ordinary Differential Equation (ODE), facilitating the use of various high-order solvers to accelerate sampling. However, although the sampling method based on differential drivers accelerates the sampling process, it ignores the time delay caused by the computational complexity of the model itself.

In this paper, we tackle the acceleration challenge from a novel perspective. Instead of concentrating solely on sampling strategies, we propose decomposing the overall image generation task into several sub-tasks, each of which can be addressed with a simpler architecture. Specifically, we decompose the generation target into multiple scales, with each scale representing a distinct level of information. The initial scale, which has the lowest resolution, contains the most fundamental information, akin to the low-frequency component in wavelet analysis. Compared to full-resolution generation, these low-resolution components can be trained or sampled more efficiently. Subsequent scales capture increasingly finer residual information between the full-resolution input and the lower-resolution components at each scale, as depicted in Fig. 1. From a deep learning perspective, residual information is often more tractable to model, enabling us to utilize a simpler architecture with fewer sampling steps and a smaller backbone to process these high-resolution residual components.

<sup>1</sup>Equal contributions.

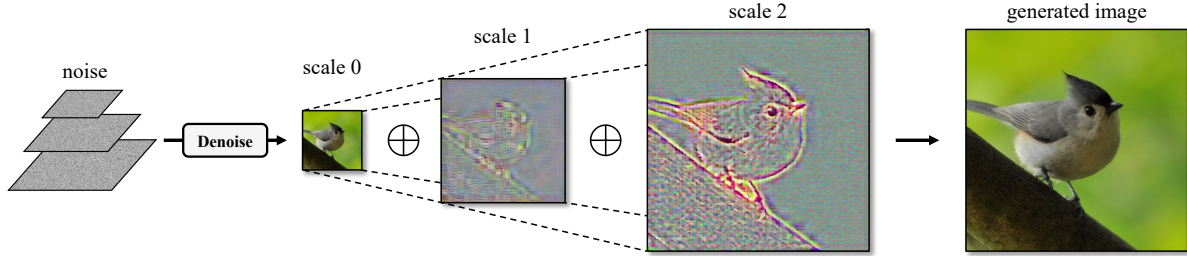


Figure 1. An illustration of MSF, where diffusion models generate hierarchical representations at multiple scales. The multi-scale representations are progressively accumulated to produce the final output. At each scale, the denoising target is derived from latents extracted by an off-the-shelf, pretrained Variational Autoencoder (VAE).

In general, we decompose a complex high-resolution generation task into two simplified stages: (1) generating a basic low-resolution component, and (2) generating multiple residual components. Our experiments demonstrate that the combined cost of these two stages is significantly lower than that of the original full-resolution generation task. The key contributions of this paper are as follows:

- We propose a hierarchical target decomposition method for diffusion models, which decomposes full-resolution inputs into a low-resolution basic component and multiple high-resolution residual components.
- We explore a multi-scale training and inference pipeline, where individual DiT backbones are responsible for generating targets at different scales.
- Our experiments demonstrate the effectiveness of MSF, showing significant improvements in computational efficiency and generation quality.

## 2. Related Work

**Diffusion-based Image Generation** Diffusion-based generative models [20, 37, 46, 48] have garnered significant attention in recent years. These models are trained to reverse the process of adding noise to a clean sample, learning to progressively denoise a noisy input. During the sampling phase, starting from random noise, the model iteratively denoises the input over multiple steps, with each step producing a progressively clearer sample, ultimately generating a high-quality image. Compared to GAN-based methods [10, 16, 23, 36, 44], diffusion models offer improved training stability and are capable of generating samples with higher fidelity. However, the iterative sampling process can be computationally intensive and time-consuming. To accelerate the training and inference of diffusion models, Latent Diffusion Models (LDM) [42] propose performing the diffusion process in the latent space of a Variational Autoencoder (VAE [27]). By leveraging the significant spatial compression provided by the VAE encoder (typically an  $8 \times 8$  downsampling rate), LDMs achieve substantial improvements in both

training and inference speed. This compression enables more efficient computation, making it feasible to scale up diffusion models to larger and more complex architectures. Following the LDM approach, a series of works [6–8, 11, 29, 39] have focused on enhancing diffusion models to generate higher-quality and higher-resolution images. These advancements aim to further improve the visual fidelity and detail in the generated outputs, pushing the boundaries of what diffusion models can achieve in terms of image quality.

**Diffusion Backbone** Diffusion-based generative models primarily focus on two model frameworks. Early works, such as [20, 42], adopted traditional U-Nets as the de-facto choice of backbone architecture. To further enhance the scalability of diffusion-based models, DiT [38] proposed using Transformers to replace the traditional U-Net, employing a vision transformer as the backbone for latent diffusion models (LDMs). MDT [15] proposes a masked latent modeling method to enhance the learning ability of internal contextual relationships within images by DPMs. U-ViT [1] treats all inputs as tokens and employs long skip connections. Building upon DiT, SiT [35] introduces an interpolation framework and explores various rectified flow configurations. FiT [34], on the other hand, investigates the potential for generating images at arbitrary resolutions and aspect ratios. FiTv2 [50] builds upon FiT with additional engineering optimizations, further improving its convergence speed and performance. In this work, building upon the traditional DiT architecture, we propose MSF, an efficient diffusion model via multi-scale latent factorization, inspired by frequency decomposition.

**Multi-Stage Diffusion Models** To generate high-fidelity visual content via diffusion models, cascaded diffusion models, also termed multi-stage diffusion models, have been introduced and broadly implemented [21, 22, 43, 45, 53]. The process begins with a base diffusion model that produces low-resolution images and cascades to generate

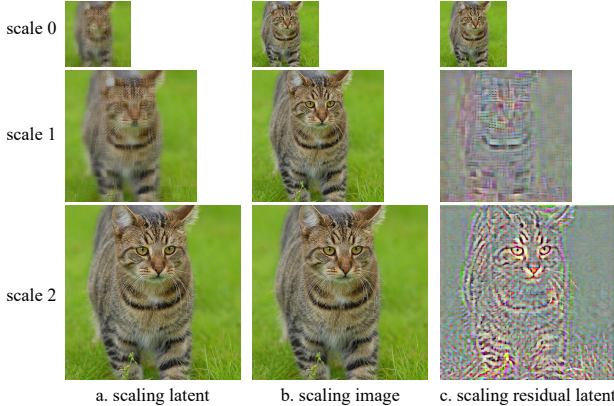


Figure 2. A comparison of different multi-scale latent factorization methods. We visualize the multi-scale latents decoded by the VAE decoder in RGB space. The method (a) operates directly in the VAE latent space. It is evident that at the smallest scale (scale 0), the reconstruction exhibits significant degeneration. The method (b) illustrates a process where the original image is first downsampled in RGB space, and the downsampled images at different scales are then passed through the VAE encoder to obtain multi-scale latents. However, this approach fails to capture hierarchical structures across scales, such as texture and high-frequency details. The method (c) shows our proposed method, which first captures the basic small-scale components, with larger-scale components obtained through residual factorization. The detailed pipeline can be found in Algorithm 1.

high-resolution visual content with a series of additional diffusion models and interpolation networks [2, 3]. Yet, within these frameworks, each stage undertakes a complete generation task, incurring considerable computational costs and time expenditures. PDD [31] has innovatively applied pyramidal discrete diffusion models to synthesize large-scale 3D scenes within resource limitations, utilizing a coarse-to-fine approach to progressively upscale generation and employ scene subdivision techniques. DoD [52] proposed enhancing diffusion models with visual priors and designed a multi-stage generation framework. The initial stage carries out standard class generation, with subsequent stages extracting visual priors by encoding the results of the preceding stage to guide the diffusion model. However, DoD’s multi-stage diffusion model maintains uniform resolution across all stages, the initial stage remains a challenge in generating high-resolution images from coarse and limited class information.

In contrast, our approach dividing the generation process into multiple scales, gradually refines finer residual details between the full-resolution input and the lower-resolution components at each scale. Compared to full-resolution generation, the multi-scale residual information is more amenable to modeling, allowing for the employment of a simpler architecture that enhances computational efficiency

in both for training and sampling.

### 3. Method

In this section, we present a comprehensive description of the proposed MSF method. First, we provide an overarching overview of MSF to contextualize its components. Subsequently, we detail the key modules of MSF as follows: (i) the extraction of multi-scale latent representations using a pretrained variational autoencoder (VAE); (ii) the multi-level diffusion module that generates latent representations at each scale; and (iii) the sampling process, which aggregates the residual latent representations from all levels to produce the final output.

#### 3.1. An Overview of MSF

Given an input image  $\mathbf{x} \in \mathbb{R}^{H \times W \times 3}$ , a multi-scale VAE encodes it into a set of tokens  $\{f_0, f_1, \dots, f_N\}$ , where each token  $f_i \in \mathbb{R}^{h_i \times w_i \times C}$  represents a distinct scale. Once the multi-scale latents  $\{f_0, f_1, \dots, f_N\}$  are obtained, a straightforward approach is to use all preceding scales to predict the ground truth latent of the current scale:

$$p(f_0, f_1, \dots, f_N) = \prod_{i=0}^N p(f_i | f_0, \dots, f_{i-1}) \quad (1)$$

where  $p(\cdot)$  indicates a diffusion-based next-scale prediction network, conditioned on the preceding scale inputs. In this paper, each  $f_i$  essentially represents a decomposition of the visual signal. To model Equ. 1 more effectively, we scale all previous scale latents to a unified scale and aggregate them together as a condition for predicting the current scale, or input prior. We will delve into this process for the input priors in Section 3.3.

#### 3.2. Multi-Scale Variational Autoencoder

Given an input image  $\mathbf{x} \in \mathbb{R}^{H \times W \times 3}$  and a pretrained VAE encoder  $\mathcal{E}$ , we can derive the latent representation  $\hat{f} \in \mathbb{R}^{h \times w \times C}$  via  $\hat{f} = \mathcal{E}(\mathbf{x})$ . Various methods are available to factorize the single-scale latent into multi-scale latents:

**Scaling Latent** A straightforward method for obtaining multi-scale latents involves scaling the latent representation  $\mathbf{v}$  using down-sampling interpolation. As shown in Fig. 2(a), when employing bilinear interpolation, the scaled latent  $f_i$  is computed as follows:

$$f_i = \text{BILINEAR}(\hat{f}, h_i, w_i) \quad (2)$$

where  $h_i$  and  $w_i$  denote the target height and width of the scaled latent.

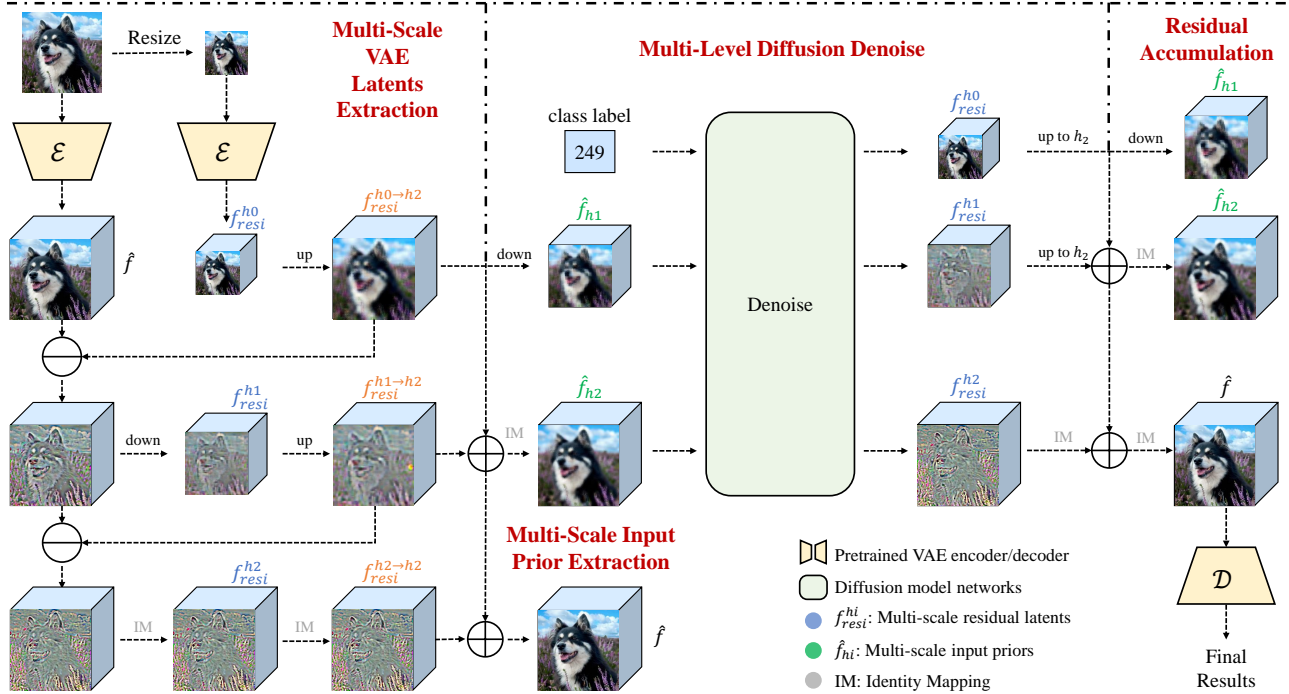


Figure 3. An overview of the proposed MSF. The figure on the left illustrates the process of extracting multi-scale residual latents  $f_{resi}^{h_i}$  using the pretrained VAE. The middle depicts the construction process of multi-scale input priors  $\hat{f}_{h_i}$  and how the diffusion model takes  $\hat{f}_{h_i}$  as input to generate the ground-truth residual latents  $f_{resi}^{h_i}$ . During inference, we first generate the residual latents  $f_{resi}^{h_i}$ , and then perform residual accumulation (illustrated in the figure on the right) to obtain the  $\hat{f}_{h_i}$ , which serves as input for the next-scale prediction.

**Scaling Image** In addition to directly scaling the latent representations using down-sampling interpolation, another approach involves scaling the input image before feeding it into the VAE encoder  $\mathcal{E}$ . As shown in Fig. 2(b), the scaled image  $\mathbf{x}_i$  and scaled latent  $f_i$  can be computed as follows:

$$\mathbf{x}_i = \text{BILINEAR}(\mathbf{x}, H_i, W_i) \quad (3)$$

$$f_i = \mathcal{E}(\mathbf{x}_i) \quad (4)$$

**Scaling Residual Latent** The aforementioned scaling methods generate small-scale latents from the original single-scale latent through direct interpolation. While this approach allows each latent at different scales to represent information from images of varying resolutions, it does not establish an explicit relationship between the generated small-scale latents. In other words, such multi-scale latents lack a hierarchical structure. For instance, some latents might capture global information, while others are more focused on local details.

To ensure the hierarchical structure of the extracted multi-scale latents, we leverage the concept of residual learning, a fundamental technique in the field of deep learning [18]. In the context of residual learning within a VAE framework, the first step involves extracting the **basic components**  $f_0$  from the latent representation  $\hat{f}$ . These ba-

sic components should capture the most fundamental, low-level information of  $\hat{f}$ , analogous to the low-frequency components in Fourier decomposition. We evaluate two methods for obtaining these basic components: (1) directly downsampling  $\hat{f}$  in the latent space, and (2) downsampling the input image first and then using the VAE latents from the downsampled image as the basic components. In our experiments, we observe that the first method—downsampling in the latent space—results in significant information loss. In contrast, the second method, which involves downsampling the input image first and then using the VAE latents from the downsampled image, preserves most of the information contained in  $\hat{f}$ . Consequently, we adopt the second method in MSF. The visualization of multi-scale residual latents is shown in Fig. 2(c).

**Multi-scale Residual Latents Extraction** Given the original latent representation  $\hat{f}$  and its primary component  $f_0$  (denoted as  $f_{resi}^{h_0}$  in Fig. 3), we first compute the residual latent at the initial scale as  $\hat{f} - \text{Up}(f_0)$ , where  $\text{Up}(\cdot)$  represents the upsampling operation employed to match the spatial dimensions of  $\hat{f}$  and  $f_0$ . To further decompose the first-scale residual latent  $\hat{f} - \text{Up}(f_0)$ , we derive its fundamental component by applying downsampling:  $f_{resi}^{h_1} =$

Down( $\hat{f} - \text{Up}(f_0)$ ). The subsequent steps follow a similar procedure. A detailed description of this process is provided in Algorithm 1. During the training phase, the extracted multi-scale residual latents  $R = \{f_{resi}^{h_i}\}_{i=0}^N$  serve as the ground truth for each scale prediction.

---

**Algorithm 1** Multi-scale Residual Latents Extraction
 

---

- 1: **Inputs:** high and low resolution image pair  $(I_h, I_l)$ , resolutions  $(h_i, w_i)_{i=0}^N$ ;
  - 2: **Encode:**  $\hat{f} = \mathcal{E}(I_h)$ ,  $f_0 = f_{resi}^{h_0} = \mathcal{E}(I_l)$ ;
  - 3: **Initialize:**  $R = \{\}$ ,  $R = R \cup \{f_{resi}^{h_0}\}$ ;
  - 4: **for**  $i = 0$  to  $N - 1$  **do**
  - 5:    $\hat{f} = \hat{f} - \text{Up}(f_{resi}^{h_i}, h_N, w_N)$ ;
  - 6:    $f_{resi}^{h_{i+1}} = \text{Down}(\hat{f}, h_{i+1}, w_{i+1})$ ;
  - 7:    $R = R \cup \{f_{resi}^{h_{i+1}}\}$ ;
  - 8: **end for**
  - 9: **Return:** multi-scale residual latents  $R$ ;
- 

---

**Algorithm 2** Multi-scale Input Prior Extraction
 

---

- 1: **Inputs:** multi-scale residual latents  $R = \{f_{resi}^{h_i}\}_{i=0}^N$ ;
  - 2: **Initialize:**  $\hat{f} = 0$ ,  $P = \{\}$ ;
  - 3: **for**  $i = 0$  to  $N - 1$  **do**
  - 4:    $f_{resi}^{h_i \rightarrow h_N} = \text{Up}(f_{resi}^{h_i}, h_N, w_N)$ ;
  - 5:    $\hat{f} = \hat{f} + f_{resi}^{h_i \rightarrow h_N}$ ;
  - 6:    $\hat{f}_{h_{i+1}} = \text{Down}(\hat{f}, h_{i+1}, w_{i+1})$ ;
  - 7:    $P = P \cup \{\hat{f}_{h_{i+1}}\}$ ;
  - 8: **end for**
  - 9: **Return:** multi-scale input prior  $P$ ;
- 

### 3.3. Multi-Scale Diffusion Loss

**Multi-scale Input Prior Extraction** In our framework, the input prior  $\hat{f}_{h_i}$  represents the cumulative latent representations from scales 0 to  $i - 1$ , facilitating a more efficient modeling of Eq. 1. Notably, the initial scale has no input prior and directly produces a low-resolution primary signal from class labels  $c$ . It is natural for the model to execute sequentially in the inference phase, whereas during the training phase, we utilize teacher-forcing to guide the model in parallel training. The process of extracting multi-scale input priors mirrors the inverse of the decomposition performed during multi-scale residual latents extraction on the original latent representation  $\hat{f}$ . Beginning at scale 0,  $\hat{f}$  accumulates residuals  $f_{resi}^{h_i}$  progressively across scales. It is important to note that these residuals must be upsampled to  $f_{resi}^{h_i \rightarrow h_N}$  to match the spatial dimensions of  $\hat{f}$ . The input prior  $\hat{f}_{h_i}$  is obtained by downsampling  $\hat{f}$ , which has integrated information from scales 0 through  $i - 1$ , to match the dimensions of the current scale. As illustrated in Fig. 3, the aggregation of latent representations across all scales enables the reconstruction of  $\hat{f}$ . However, the extraction of input priors does not necessitate the inclusion of the final

latent representation. The detailed procedure for obtaining the multi-scale input prior  $P = \{\hat{f}_{h_i}\}_{i=1}^N$  during the training phase is elaborated in Algorithm 2.

**Flow-Based Next-Scale Prediction** After obtaining the input prior according to Algorithm 2, it serves as the condition to generate the residual target on the current scale. Specifically, we use the Rectified Flow [30] diffusion model due to its stability during training and fast inference speed. This approach translates the predicted next-scale information to align with the ground truth data distributed in the latent space. The rectified flow model aims to learn the velocity field  $v$ , which transforms random noise  $\mathbf{z}_0 \sim \mathcal{N}(0, 1)$  into the ground truth distribution  $f_{resi}^{h_i} \sim \pi_{data}$ :

$$\mathcal{L} = \sum_{i=0}^N \int_0^1 \mathbb{E}[||f_{resi}^{h_i} - \mathbf{z}_0 - v_\theta(\mathbf{z}_t, t|f_{resi}^{h_{i-1}})||^2] dt \quad (5)$$

where  $N$  is the number of total scales, and  $\mathbf{z}_t = t \cdot f_{resi}^{h_i} + (1-t) \cdot \mathbf{z}_0$ . After trained, we use an ODE function to sample  $f_{resi}^{h_i}$  at different scale during inference:

$$d\mathbf{z}_t = v_\theta(\mathbf{z}_t, t|c_i, f_{resi}^{h_{i-1}}) dt \quad (6)$$

### 3.4. Multi-Scale Accumulate Sampling

The sampling process begins with class label  $c$  and computes the residual latent representation  $f_{resi}^{h_i}$  for each scale  $i$  in a manner similar to autoregressive methods. The residual latents are accumulated to obtain the final generated image’s latent representation  $\hat{f}$ . Specifically, the initial scale generates a low-resolution primary signal  $f_{resi}^{h_0}$  based on class labels  $c$ , while subsequent scales produce high-resolution residual signals conditioned on both input prior  $\hat{f}_{h_i}$  and class label  $c$ . The computation result  $f_{resi}^{h_i}$  at each scale is upsampled to the size of  $(h_N, w_N)$  and accumulated into  $\hat{f}$ . And then  $\hat{f}$ , containing the cumulative results of all current scales, is downsampled to  $(h_{i+1}, w_{i+1})$  and serves as the input prior for the next scale. After adding the residual latent representation of the last scale, the generated image can be obtained by decoding  $\hat{f}$  with VAE decoder. The complete procedure for sampling is detailed in Algorithm 3.

## 4. Experiments

In this section, we conduct experiments on the ImageNet [12] dataset at a resolution of  $256 \times 256$ . We first evaluate both the Fréchet Inception Distance (FID) and Inception Score (IS) using standard evaluation protocols. Subsequently, we compare the inference time of MSF with those of other baseline methods, demonstrating the effectiveness of MSF. We also analyze the performance of MSF with several detailed ablation studies.

---

**Algorithm 3** Autoregressive sampling

---

```
1: Inputs: class label  $c$ , resolutions  $(h_i, w_i)_{i=0}^N$ ;  
2: Initialize:  $\hat{f} = 0$ ;  
3: for  $i = 0$  to  $N$  do  
4:   if  $i == 0$  then  
5:      $f_{resi}^{h_i} \sim v_\theta(\mathbf{z}_t, t|c)$ ;  
6:   else  
7:      $f_{resi}^{h_i} \sim v_\theta(\mathbf{z}_t, t|c, \hat{f}_{h_i})$ ;  
8:   end if  
9:    $\hat{f} = \hat{f} + \text{Up}(f_{resi}^{h_i}, h_N, w_N)$ ;  
10:  if  $i < N$  then  
11:     $\hat{f}_{h_{i+1}} = \text{Down}(\hat{f}, h_{i+1}, w_{i+1})$ ;  
12:  end if  
13: end for  
14: Decode:  $\hat{I}_h = \mathcal{D}(\hat{f})$ ;  
15: Return: generated high-resolution image  $\hat{I}_h$ ;
```

---

### 4.1. Training Details

We train diffusion models using the ImageNet 2012 training dataset. Following Stable Diffusion [42], we employ a VAE encoder with a downsampling ratio of 8 to extract latent representations of input images. For generating images at a resolution of  $256 \times 256$ , we set the number of scales as 2: the first scale is set to  $192 \times 192$  and the second to  $256 \times 256$ . During training, we follow the scaling guidelines from [17], setting the batch size to 2560 and the learning rate to  $3 \times 10^{-4}$ . The first scale is trained for 400k iterations, while the second scale requires fewer iterations (250k), as it only needs to model residual information. We also plot the training loss at each scale in Fig. 4. The loss at scale 2 is much lower than that at scale 1, as mentioned earlier. This is because the residual information is easier to model and optimize.

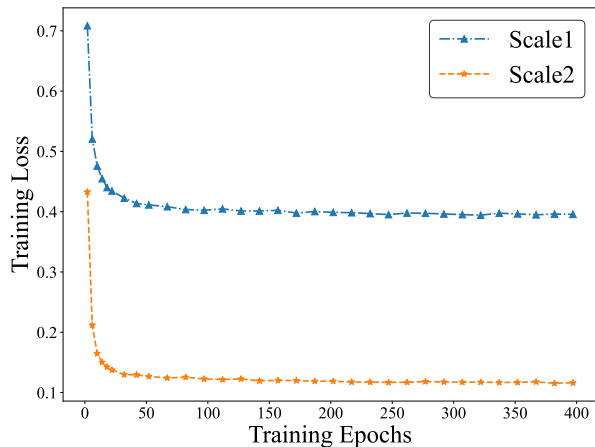


Figure 4. The Training Loss at Each Scale. The loss at scale 2 is significantly lower than that of scale 1 because scale 2 only models the residual latents, which are easier to optimize.

Regarding network architecture, the model for stage 1 generation has a depth of 18, a width of 1152, and a total of 435.9M parameters. For stage 2, the network has a depth of 10, a width of 1280, and 331.2M parameters. The combined parameters of the stage 1 and stage 2 networks total 767.1M, comparable to those of DiT-XL.

### 4.2. Results on ImageNet $256 \times 256$

We evaluate MSF using several standard metrics, including Fréchet Inception Distance (FID), Inception Score (IS), Precision, and Recall. For a fair comparison, we adopt evaluation scripts from ADM [13] and report results on 50K generated samples across 1000 ImageNet categories. We set the sampling steps for the two scales to 100 and 50, respectively, and the classifier-free guidance scales to 1.4 and 1.0 (i.e., without CFG). As shown in Table 1, MSF achieves an FID of 2.2 and an IS of 254.73, outperforming DiT with comparable model parameters. Additionally, the inference time of MSF are  $2 \times$  times lower than those of DiT. We also provide visualizations of samples generated by MSF in Fig. 5.

## 5. Analysis and Discuss

**Effects of Classifier-Free Guidance Scale** Classifier-free guidance [19] is a core technique to enhance the generative quality of diffusion models by interpolating between conditional and unconditional outputs:

$$\hat{v} = v_\theta(\mathbf{z}_t, t|\emptyset) + w \cdot (v_\theta(\mathbf{z}_t, t|c_i) - v_\theta(\mathbf{z}_t, t|\emptyset)) \quad (7)$$

where  $\emptyset$  represents the null class, corresponding to the unconditional outputs.

We evaluate the outputs of each scale under varying classifier-free guidance (CFG) scales individually, as shown in Table 2 and Table 3. The CFG primarily impacts the performance of scale 1 generation, while scale 2 achieves satisfactory results even without CFG. Since CFG requires doubling the forward passes of the inputs and introduces additional inference costs, we omit CFG for scale 2 generation in our experiments.

**Effects of Sampling Steps** Diffusion models are well-known for generating clean images from random noise through multi-step denoising, where the number of steps significantly influences generative quality. Similar to the classifier-free guidance scale, we evaluate the impact of sampling steps on MSF across different scales. As shown in Table 4 and Table 5, scale 1 achieves optimal generative performance around 100 sampling steps. For scale 2, significantly fewer steps are required compared to scale 1, as it only needs to generate residual information. When varying the sampling steps from 10 to 100, the FID-5K metric fluctuates by only 0.05, demonstrating robust performance.



Table 1. Quantitative Comparison of Class-Conditional Generative Methods on ImageNet ( $256\times 256$ ). In this comparison, “ $\downarrow$ ” indicates that lower values are preferable, while “ $\uparrow$ ” indicates that higher values are better. We report results on Fréchet Inception Distance (FID), Inception Score (IS), Precision (Pre), and Recall (Rec). Additionally, we compare the inference time costs between DiT and MSF, measured on a single A800 GPU with a batch size of 64.

Model	Para	FID $\downarrow$	IS $\uparrow$	Pre $\uparrow$	Rec $\uparrow$	Time
BigGAN [4]	112M	6.95	224.5	0.89	0.38	—
GigaGAN [23]	569M	3.45	225.5	0.84	0.61	—
StyleGan-XL [44]	166M	2.30	265.1	0.78	0.53	—
MaskGIT [5]	227M	6.18	182.1	0.80	0.51	—
VQVAE-2 [41]	13.5B	31.11	$\sim 45$	0.36	0.57	—
VQGAN [14]	1.4B	15.78	74.3	—	—	—
ViTVQ [51]	1.7B	4.17	175.1	—	—	—
ADM [13]	554M	10.94	101.0	0.69	0.63	—
ADM-G [13]	554M	4.59	186.7	0.82	0.52	—
VDM++ [26]	2B	2.12	267.7	—	—	—
CDM [22]	—	4.88	158.7	—	—	—
LDM-8-G [42]	395M	7.76	209.52	0.84	0.35	—
LDM-4-G [42]	400M	3.60	247.7	—	—	—
GIVT [49]	304M	5.67	-	0.75	0.59	—
DiT-L/2 [38]	458M	5.02	167.2	0.75	0.57	—
DiT-XL/2 [38]	675M	2.27	278.2	0.83	0.57	145
MSF(cfg=1.4)	767M	2.2	254.7	0.80	0.60	68
MSF(cfg=1.5)	767M	2.38	283.2	0.83	0.6	68

CFG	1.0	1.1	1.2	1.3	1.4	1.5
FID-5K	17.19	11.09	7.69	5.96	5.33	5.50

Table 2. With the classifier-free guidance (CFG) scale for scale 2 fixed at 1.0, we evaluate the FID-5K under different CFG for scale 1. The FID achieves the best results at 1.4.

CFG	1.0	1.1	1.2	1.3	1.4
FID-5K	5.34	5.33	5.32	5.32	5.31

Table 3. With the classifier-free guidance (CFG) scale for scale 1 fixed at 1.4, we evaluate the FID-5K under different CFG values for scale 2. The FID-5K metric shows no significant differences across varying CFG values, so we use CFG=1.0 in our experiments (i.e., no CFG for scale 2) to achieve a  $2\times$  speedup in sampling.

step	25	50	100	125	200
FID-5K	6.61	5.57	5.34	5.32	5.35

Table 4. With the sampling steps for scale 2 fixed at 50, we evaluate the FID-5K under different sampling steps for scale 1. The FID achieves better results at 100 and 125 sampling steps.

step	10	20	30	40	50	100
FID-5K	5.37	5.32	5.32	5.33	5.34	5.35

Table 5. With the sampling steps for scale 1 fixed at 100, we evaluate the FID-5K under different sampling steps for scale 2. Scale 2 requires only half the number of steps compared to scale 1 and demonstrates greater robustness when the steps are reduced to fewer values (e.g., 10).

## 6. Conclusion

In this paper, we proposed a versatile and efficient image generation framework that decomposes the full-resolution image generation process into a multi-scale, progressive hierarchy. This factorized approach enables the generation of complex high-resolution images by training transformer-based diffusion models to sequentially produce hierarchical latents. Each scale within the hierarchy captures distinct image details, with the framework learning both a fundamental low-resolution component and several residual high-resolution components. This structure enables the use of a smaller backbone network for each component compared to conventional full-resolution image generation models, leading to substantial efficiency gains without compromising output quality. Through extensive experiments, we demonstrated that this progressive, multi-scale factorization approach enhances the generative quality, achieving higher fi-

delity with fewer computational resources than traditional methods. The empirical results indicate that MSF achieves state-of-the-art performance on key benchmarks, validating the framework’s effectiveness and efficiency in high-resolution image synthesis.

## References

- [1] Fan Bao, Shen Nie, Kaiwen Xue, Yue Cao, Chongxuan Li, Hang Su, and Jun Zhu. All are worth words: A vit backbone for diffusion models. In *Proceedings of the IEEE/CVF conference on computer vision and pattern recognition*, pages 22669–22679, 2023. 2
- [2] Andreas Blattmann, Tim Dockhorn, Sumith Kulal, Daniel Mendelevitch, Maciej Kilian, Dominik Lorenz, Yam Levi, Zion English, Vikram Voleti, Adam Letts, et al. Stable video diffusion: Scaling latent video diffusion models to large datasets. *arXiv preprint arXiv:2311.15127*, 2023. 1, 3
- [3] Andreas Blattmann, Robin Rombach, Huan Ling, Tim Dockhorn, Seung Wook Kim, Sanja Fidler, and Karsten Kreis. Align your latents: High-resolution video synthesis with latent diffusion models. In *Proceedings of the IEEE/CVF Conference on Computer Vision and Pattern Recognition*, pages 22563–22575, 2023. 1, 3
- [4] Andrew Brock, Jeff Donahue, and Karen Simonyan. Large scale gan training for high fidelity natural image synthesis. *ArXiv*, abs/1809.11096, 2018. 8
- [5] Huiwen Chang, Han Zhang, Lu Jiang, Ce Liu, and William T. Freeman. Maskgit: Masked generative image transformer. *2022 IEEE/CVF Conference on Computer Vision and Pattern Recognition (CVPR)*, pages 11305–11315, 2022. 8
- [6] Junsong Chen, Jincheng Yu, Chongjian Ge, Lewei Yao, Enze Xie, Yue Wu, Zhongdao Wang, James Kwok, Ping Luo, Huchuan Lu, et al. Pixart-alpha: Fast training of diffusion transformer for photorealistic text-to-image synthesis. *arXiv preprint arXiv:2310.00426*, 2023. 2
- [7] Junsong Chen, Chongjian Ge, Enze Xie, Yue Wu, Lewei Yao, Xiaozhe Ren, Zhongdao Wang, Ping Luo, Huchuan Lu, and Zhenguo Li. Pixart- $\sigma$ : Weak-to-strong training of diffusion transformer for 4k text-to-image generation. *arXiv preprint arXiv:2403.04692*, 2024.
- [8] Junsong Chen, Yue Wu, Simian Luo, Enze Xie, Sayak Paul, Ping Luo, Hang Zhao, and Zhenguo Li. Pixart- $\delta$ : Fast and controllable image generation with latent consistency models. *arXiv preprint arXiv:2401.05252*, 2024. 2
- [9] Nanxin Chen, Yu Zhang, Heiga Zen, Ron J. Weiss, Mohammad Norouzi, Najim Dehak, and William Chan. Wavegrad 2: Iterative refinement for text-to-speech synthesis. *ArXiv*, abs/2106.09660, 2021. 1
- [10] Xi Chen, Yan Duan, Rein Houthoofd, John Schulman, Ilya Sutskever, and Pieter Abbeel. Infogan: Interpretable representation learning by information maximizing generative adversarial nets. *Advances in neural information processing systems*, 29, 2016. 2
- [11] Xiaoliang Dai, Ji Hou, Chih-Yao Ma, Sam Tsai, Jialiang Wang, Rui Wang, Peizhao Zhang, Simon Vandenhende, Xiaofang Wang, Abhimanyu Dubey, et al. Emu: Enhancing image generation models using photogenic needles in a haystack. *arXiv preprint arXiv:2309.15807*, 2023. 1, 2
- [12] Jia Deng, Wei Dong, Richard Socher, Li-Jia Li, Kai Li, and Li Fei-Fei. Imagenet: A large-scale hierarchical image database. In *2009 IEEE conference on computer vision and pattern recognition*, pages 248–255. Ieee, 2009. 5
- [13] Prafulla Dhariwal and Alexander Nichol. Diffusion models beat gans on image synthesis. *Advances in neural information processing systems*, 34:8780–8794, 2021. 6, 8
- [14] Patrick Esser, Robin Rombach, and Björn Ommer. Taming transformers for high-resolution image synthesis. In *Proceedings of the IEEE/CVF Conference on Computer Vision and Pattern Recognition*, pages 12873–12883, 2021. 8
- [15] Shanghua Gao, Pan Zhou, Ming-Ming Cheng, and Shuicheng Yan. Masked diffusion transformer is a strong image synthesizer. In *Proceedings of the IEEE/CVF International Conference on Computer Vision*, pages 23164–23173, 2023. 2
- [16] Ian Goodfellow, Jean Pouget-Abadie, Mehdi Mirza, Bing Xu, David Warde-Farley, Sherjil Ozair, Aaron Courville, and Yoshua Bengio. Generative adversarial nets. *Advances in neural information processing systems*, 27, 2014. 2
- [17] P Goyal. Accurate, large minibatch sg d: training imagenet in 1 hour. *arXiv preprint arXiv:1706.02677*, 2017. 6
- [18] Kaiming He, Xiangyu Zhang, Shaoqing Ren, and Jian Sun. Deep residual learning for image recognition. In *Proceedings of the IEEE conference on computer vision and pattern recognition*, pages 770–778, 2016. 4
- [19] Jonathan Ho and Tim Salimans. Classifier-free diffusion guidance. *arXiv preprint arXiv:2207.12598*, 2022. 6
- [20] Jonathan Ho, Ajay Jain, and Pieter Abbeel. Denoising diffusion probabilistic models. *Advances in neural information processing systems*, 33:6840–6851, 2020. 2
- [21] Jonathan Ho, William Chan, Chitwan Saharia, Jay Whang, Ruiqi Gao, Alexey Gritsenko, Diederik P Kingma, Ben Poole, Mohammad Norouzi, David J Fleet, et al. Imagen video: High definition video generation with diffusion models. *arXiv preprint arXiv:2210.02303*, 2022. 1, 2
- [22] Jonathan Ho, Chitwan Saharia, William Chan, David J Fleet, Mohammad Norouzi, and Tim Salimans. Cascaded diffusion models for high fidelity image generation. *Journal of Machine Learning Research*, 23(47):1–33, 2022. 2, 8
- [23] Minguk Kang, Jun-Yan Zhu, Richard Zhang, Jaesik Park, Eli Shechtman, Sylvain Paris, and Taesung Park. Scaling up gans for text-to-image synthesis. In *Proceedings of the IEEE/CVF Conference on Computer Vision and Pattern Recognition*, pages 10124–10134, 2023. 2, 8
- [24] Heeseung Kim, Sungwon Kim, and Sungroh Yoon. Guided-tts: A diffusion model for text-to-speech via classifier guidance. In *International Conference on Machine Learning*, 2021. 1
- [25] Sanghwan Kim, Hao Tang, and Fisher Yu. Distilling ode solvers of diffusion models into smaller steps. In *Proceedings of the IEEE/CVF Conference on Computer Vision and Pattern Recognition*, pages 9410–9419, 2024. 1

- [26] Diederik Kingma and Ruiqi Gao. Understanding diffusion objectives as the elbo with simple data augmentation. *Advances in Neural Information Processing Systems*, 36, 2024. 8
- [27] Diederik P Kingma. Auto-encoding variational bayes. *arXiv preprint arXiv:1312.6114*, 2013. 2
- [28] Zhifeng Kong, Wei Ping, Jiayi Huang, Kexin Zhao, and Bryan Catanzaro. Diffwave: A versatile diffusion model for audio synthesis. In *International Conference on Learning Representations*. 1
- [29] Bingchen Liu, Ehsan Akhgari, Alexander Visseratin, Aleks Kamko, Linmiao Xu, Shivam Shrirao, Joao Souza, Suhail Doshi, and Daiqing Li. Playground v3: Improving text-to-image alignment with deep-fusion large language models. *arXiv preprint arXiv:2409.10695*, 2024. 1, 2
- [30] Xingchao Liu, Chengyue Gong, et al. Flow straight and fast: Learning to generate and transfer data with rectified flow. In *The Eleventh International Conference on Learning Representations*. 5
- [31] Yuheng Liu, Xinke Li, Xueting Li, Lu Qi, Chongshou Li, and Ming-Hsuan Yang. Pyramid diffusion for fine 3d large scene generation. *arXiv preprint arXiv:2311.12085*, 2023. 3
- [32] Cheng Lu, Yuhao Zhou, Fan Bao, Jianfei Chen, Chongxuan Li, and Jun Zhu. Dpm-solver++: Fast solver for guided sampling of diffusion probabilistic models. *arXiv preprint arXiv:2211.01095*, 2022. 1
- [33] Cheng Lu, Yuhao Zhou, Fan Bao, Jianfei Chen, Chongxuan Li, and Jun Zhu. Dpm-solver: A fast ode solver for diffusion probabilistic model sampling in around 10 steps. *Advances in Neural Information Processing Systems*, 35:5775–5787, 2022. 1
- [34] Zeyu Lu, Zidong Wang, Di Huang, Chengyue Wu, Xihui Liu, Wanli Ouyang, and Lei Bai. Fit: Flexible vision transformer for diffusion model. *arXiv preprint arXiv:2402.12376*, 2024. 1, 2
- [35] Nanye Ma, Mark Goldstein, Michael S Albergo, Nicholas M Boffi, Eric Vanden-Eijnden, and Saining Xie. Sit: Exploring flow and diffusion-based generative models with scalable interpolant transformers. *arXiv preprint arXiv:2401.08740*, 2024. 2
- [36] Mehdi Mirza. Conditional generative adversarial nets. *arXiv preprint arXiv:1411.1784*, 2014. 2
- [37] Alexander Quinn Nichol and Prafulla Dhariwal. Improved denoising diffusion probabilistic models. In *International conference on machine learning*, pages 8162–8171. PMLR, 2021. 2
- [38] William Peebles and Saining Xie. Scalable diffusion models with transformers. In *Proceedings of the IEEE/CVF International Conference on Computer Vision*, pages 4195–4205, 2023. 1, 2, 8
- [39] Dustin Podell, Zion English, Kyle Lacey, Andreas Blattmann, Tim Dockhorn, Jonas Müller, Joe Penna, and Robin Rombach. Sdxl: Improving latent diffusion models for high-resolution image synthesis. *arXiv preprint arXiv:2307.01952*, 2023. 1, 2
- [40] Vadim Popov, Ivan Vovk, Vladimir Gogoryan, Tasnima Sadekova, and Mikhail A. Kudinov. Grad-tts: A diffusion probabilistic model for text-to-speech. In *International Conference on Machine Learning*, 2021. 1
- [41] Ali Razavi, Aäron van den Oord, and Oriol Vinyals. Generating diverse high-fidelity images with vq-vae-2. In *Neural Information Processing Systems*, 2019. 8
- [42] Robin Rombach, Andreas Blattmann, Dominik Lorenz, Patrick Esser, and Björn Ommer. High-resolution image synthesis with latent diffusion models. In *Proceedings of the IEEE/CVF conference on computer vision and pattern recognition*, pages 10684–10695, 2022. 2, 6, 8
- [43] Chitwan Saharia, William Chan, Saurabh Saxena, Lala Li, Jay Whang, Emily L Denton, Kamyar Ghasemipour, Raphael Gontijo Lopes, Burcu Karagol Ayan, Tim Salimans, et al. Photorealistic text-to-image diffusion models with deep language understanding. *Advances in neural information processing systems*, 35:36479–36494, 2022. 1, 2
- [44] Axel Sauer, Katja Schwarz, and Andreas Geiger. Stylegan-xl: Scaling stylegan to large diverse datasets. In *ACM SIGGRAPH 2022 conference proceedings*, pages 1–10, 2022. 2, 8
- [45] Uriel Singer, Adam Polyak, Thomas Hayes, Xi Yin, Jie An, Songyang Zhang, Qiyuan Hu, Harry Yang, Oron Ashual, Oran Gafni, et al. Make-a-video: Text-to-video generation without text-video data. In *The Eleventh International Conference on Learning Representations*. 1, 2
- [46] Jiaming Song, Chenlin Meng, and Stefano Ermon. Denoising diffusion implicit models. *arXiv preprint arXiv:2010.02502*, 2020. 2
- [47] Yang Song, Jascha Sohl-Dickstein, Diederik P Kingma, Abhishek Kumar, Stefano Ermon, and Ben Poole. Score-based generative modeling through stochastic differential equations. *arXiv preprint arXiv:2011.13456*, 2020. 1
- [48] Yang Song, Jascha Sohl-Dickstein, Diederik P Kingma, Abhishek Kumar, Stefano Ermon, and Ben Poole. Score-based generative modeling through stochastic differential equations. *arXiv preprint arXiv:2011.13456*, 2020. 2
- [49] Michael Tschannen, Cian Eastwood, and Fabian Mentzer. Givit: Generative infinite-vocabulary transformers. In *European Conference on Computer Vision*, pages 292–309. Springer, 2025. 8
- [50] Zidong Wang, Zeyu Lu, Di Huang, Cai Zhou, Wanli Ouyang, et al. Fitv2: Scalable and improved flexible vision transformer for diffusion model. *arXiv preprint arXiv:2410.13925*, 2024. 1, 2
- [51] Jiahui Yu, Xin Li, Jing Yu Koh, Han Zhang, Ruoming Pang, James Qin, Alexander Ku, Yuanzhong Xu, Jason Baldridge, and Yonghui Wu. Vector-quantized image modeling with improved vqgan. *ArXiv*, abs/2110.04627, 2021. 8
- [52] Xiaoyu Yue, Zidong Wang, Zeyu Lu, Shuyang Sun, Meng Wei, Wanli Ouyang, Lei Bai, and Luping Zhou. Diffusion models need visual priors for image generation. *arXiv preprint arXiv:2410.08531*, 2024. 3
- [53] David Junhao Zhang, Jay Zhangjie Wu, Jia-Wei Liu, Rui Zhao, Lingmin Ran, Yuchao Gu, Difei Gao, and Mike Zheng Shou. Show-1: Marrying pixel and latent diffusion models for text-to-video generation. *International Journal of Computer Vision*, pages 1–15, 2024. 1, 2

- [54] Kaiwen Zheng, Cheng Lu, Jianfei Chen, and Jun Zhu. Dpm-solver-v3: Improved diffusion ode solver with empirical model statistics. *Advances in Neural Information Processing Systems*, 36:55502–55542, 2023. [1](#)
- [55] Zhenyu Zhou, Defang Chen, Can Wang, and Chun Chen. Fast ode-based sampling for diffusion models in around 5 steps. In *Proceedings of the IEEE/CVF Conference on Computer Vision and Pattern Recognition*, pages 7777–7786, 2024. [1](#)

# Supplementary Material for MSF: Efficient Diffusion Model Via Multi-Scale Latent Factorize

## 7. More Visualizations

In Figs. 6, 7, 8, 9, 10, 11 and 12, we present additional samples to showcase the performance of MSF. It is important to emphasize that these images were not cherry-picked; rather, they were generated as  $256 \times 256$  images in a single random batch for each class label, highlighting the generation success rate of MSF.



Figure 6. A random batch of generated  $256 \times 256$  images for class label 980 (not cherry-picked).



Figure 7. A random batch of generated 256×256 images for class label 330 (not cherry-picked).

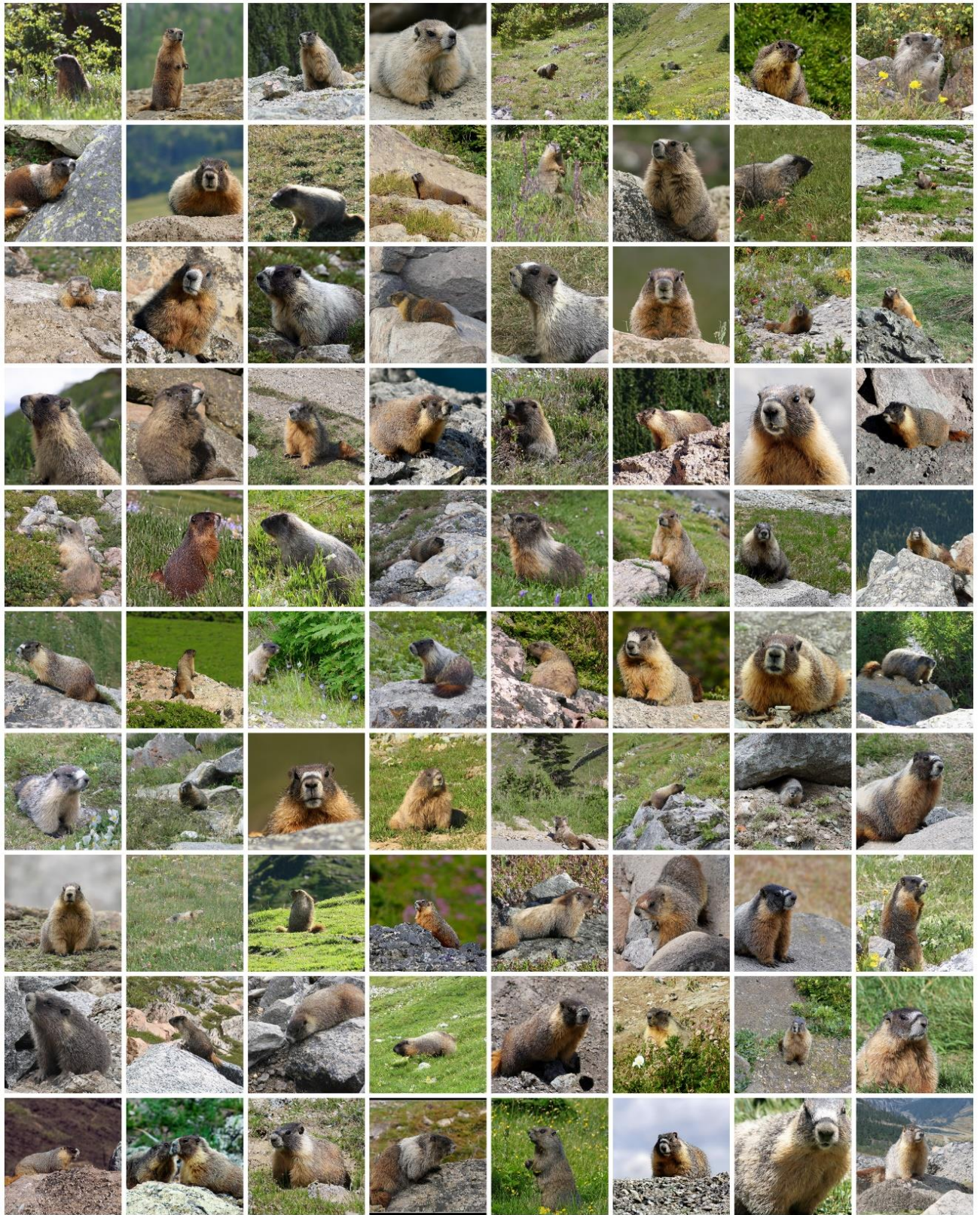


Figure 8. A random batch of generated 256×256 images for class label 336 (not cherry-picked).



Figure 9. A random batch of generated 256×256 images for class label 497 (not cherry-picked).



Figure 10. A random batch of generated 256x256 images for class label 538 (not cherry-picked).

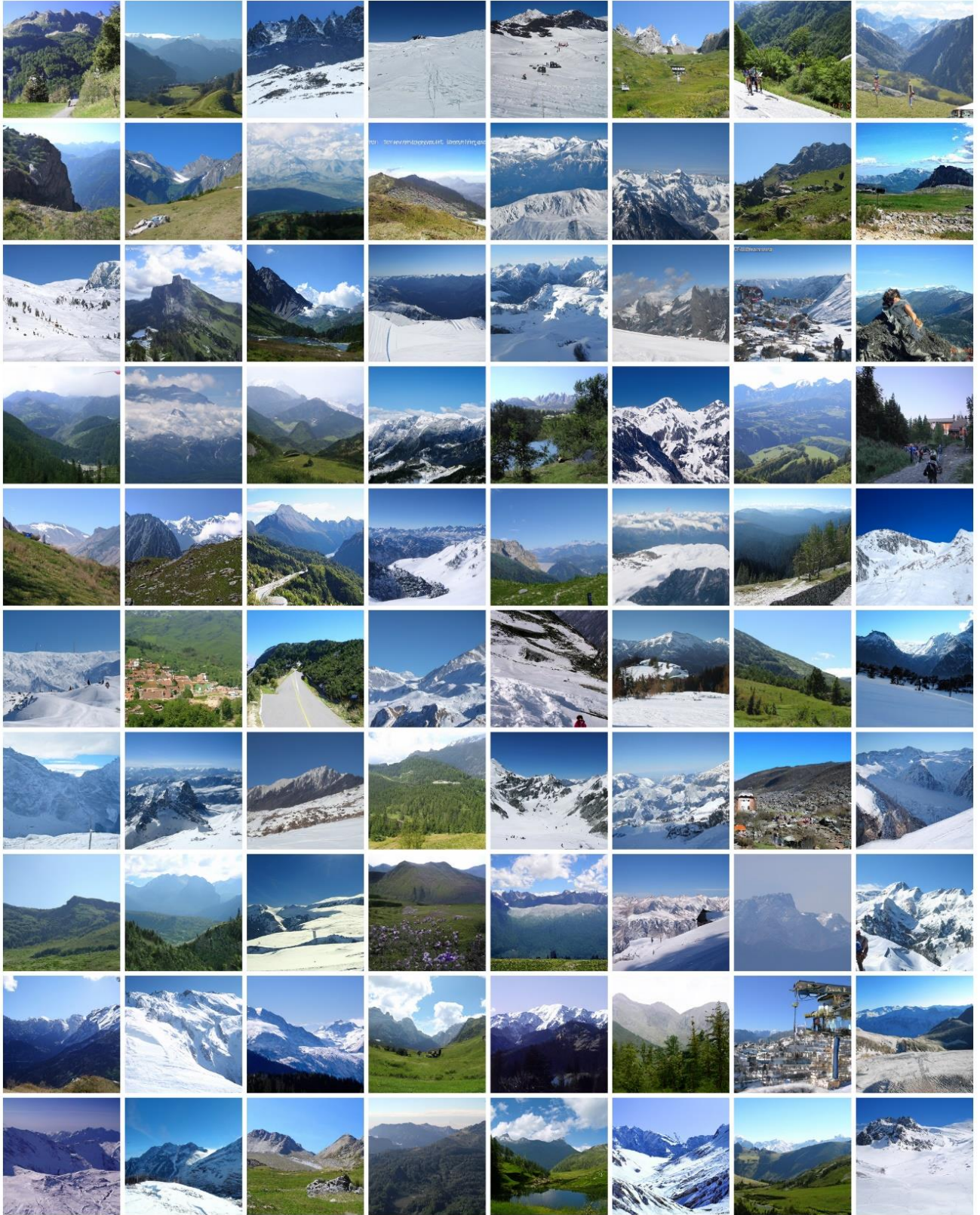


Figure 11. A random batch of generated 256x256 images for class label 970 (not cherry-picked).

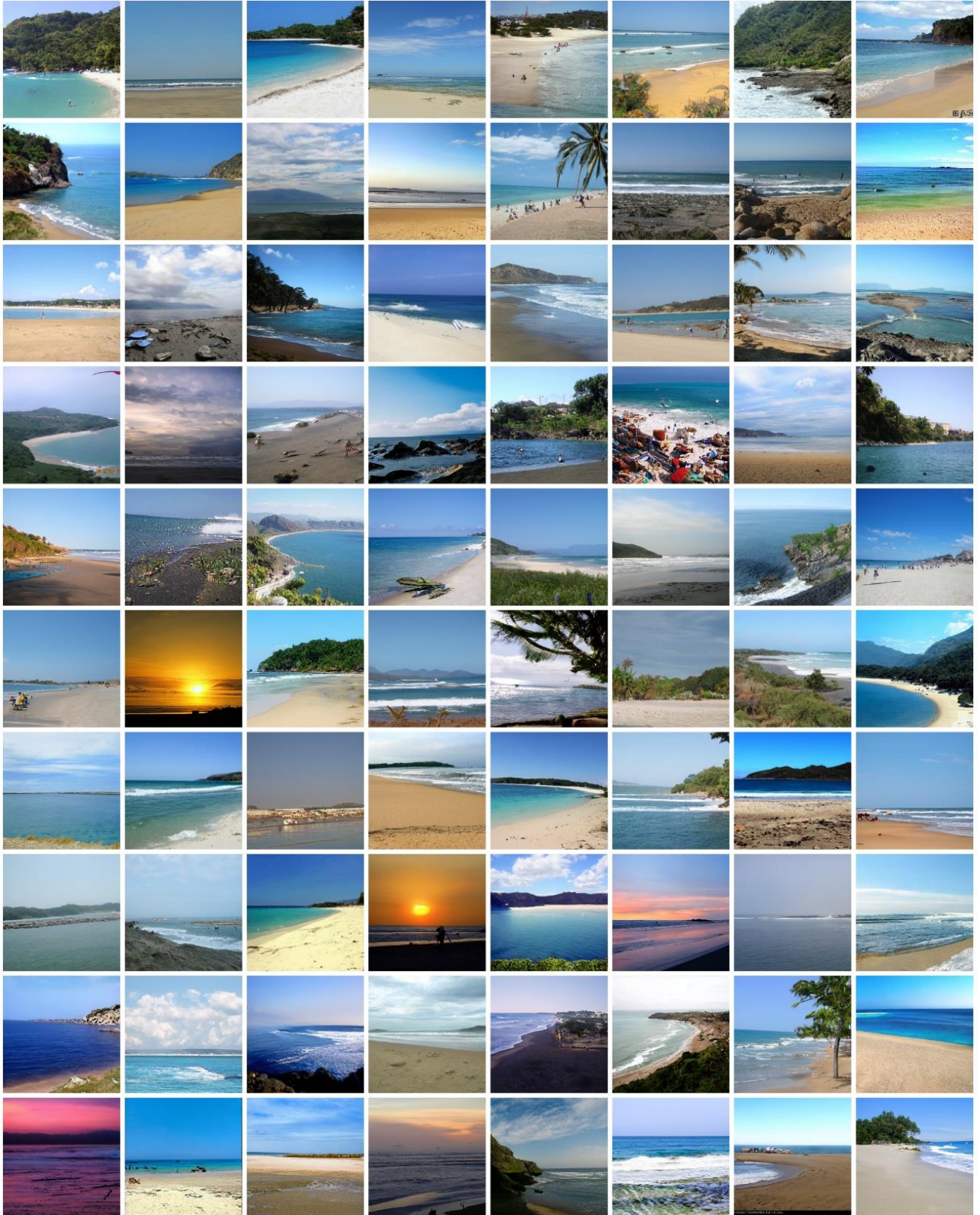


Figure 12. A random batch of generated 256x256 images for class label 978 (not cherry-picked).